Metasurface-Integrated Buried-Heterostructure Quantum Cascade Lasers for Programmable Directional Lasing Emissions

Zerui Liu[1], Kangqi Fu[2]

[1]*Department of Electrical and Computer Engineering, University of Wisconsin-Madison, 1415 Engineering Dr., Madison WI 53706, USA*
[2]*Applied Mathematics, Engineering and Physics, University of Wisconsin-Madison, 480 Lincoln Dr., Madison WI 53706, USA*

1. Introduction

Buried-heterostructure (BH) quantum cascade lasers (QCL) are widely used across various industries such as optical sensing, free-space communication and ultra-compact light detection and ranging (LiDAR). However, the method of greatly improving the performance of the laser through internal design has entered a bottleneck period, gradually chugging. The emerging artificial sheet material with sub-wavelength thickness named metasurface provides an extremely effective method to enhance the quality of the beam of lasers. Here, a novel hybrid laser system is presented by combining the BH-QCLs and a diffractive metalens consisting of cylindrical nanorods. The BH-QCLs emitting in the mid-infrared (IR) (λ = 4.3 μm) acts as the light source inside the hybrid system. The metalens consist of carefully arranged nanorods that are supposed to collimate and steer the beam produced by BH-QCLs.

2. Light source

COMSOL are being used to design a $4\mu m$-wide BH laser device producing $4\ \mu m$ light. The near-field distribution is shown in figure 1. This device can produce light at $4.3\ \mu m$. The basic parameters of the beam are extracted from COMSOL and input into FDTD as the light source.

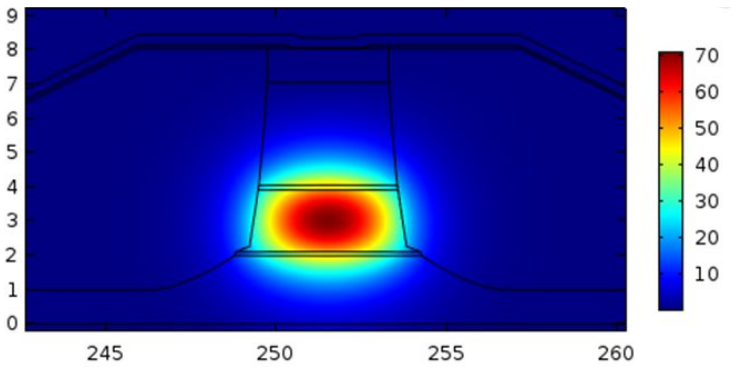

Figure 1. Fundamental mode of ~4 μm-wide BH device

3. Metalens designed for plane wave

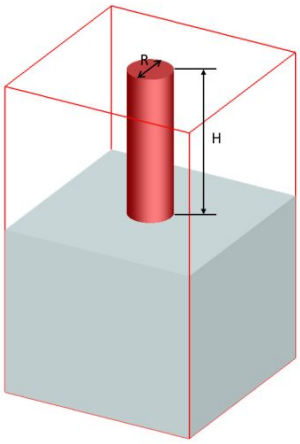

Figure 2. Schematic of unit cell of nanorib array. R and H means radius and height of nanorib, respectively.

Each unit cell inside metalens consists of one rod and square substrate. Based on the wavelength of the $4.3\ \mu m$ light source, the Si is chosen as the materials of nanorod and substrate due to the high transmission in the mid-infrared region. By varying the value of radius and height of the rod, the effective refractive index can control. Thus, waves experiencing the metalens are manipulated by carefully arranging nanorods with different radius or height.

In order to achieve a high-quality spotlight effect, there are two requirements that need to be satisfied. Firstly, no matter how the radius and height of the nanorod change, it must ensure high transmittance. Then the phase change of 2π over the whole metalens must be satisfied. Below are the distribution of phase and transmission in terms of radius and height. As we can see from figure 2, when the height of nanorod is $2.4\mu m$, the transmission fluctuates around 0.8 and then the phase change is over 2π over the whole range at the same time.

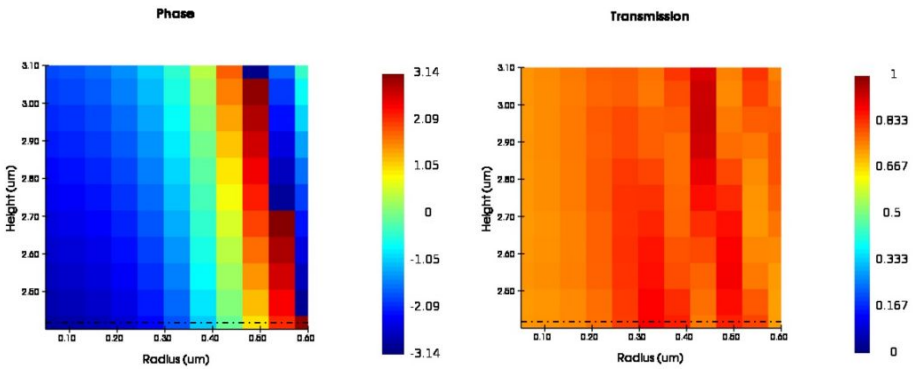

Figure 3. The 2D distribution of phase and transmission in term of radius and height.

The relationships among phase, transmission, and radius at the same height, $2.4\ \mu m$, are shown below.

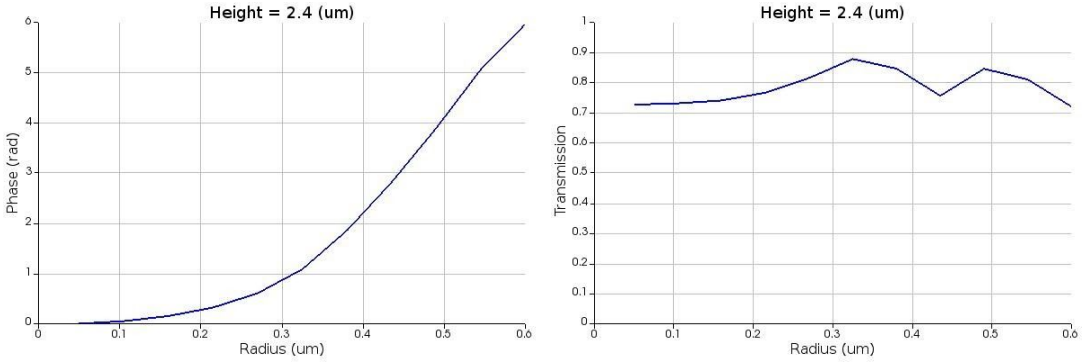

Figure 4. Plots of relation relationships among phase, transmission, and radius at the same height, $2.4\mu m$.

The lens equation for converging plane waves with target phase is shown below.

$$\varphi(x,y) = \frac{2\pi}{\lambda}\left(f - \sqrt{f^2 + x^2 + y^2}\right)$$

where

$\lambda = 4.3\mu m$

φ : *phase on the metalens surface*

f : *focal length*

x, y : *spatial coordinates with respect to the center of the lens*

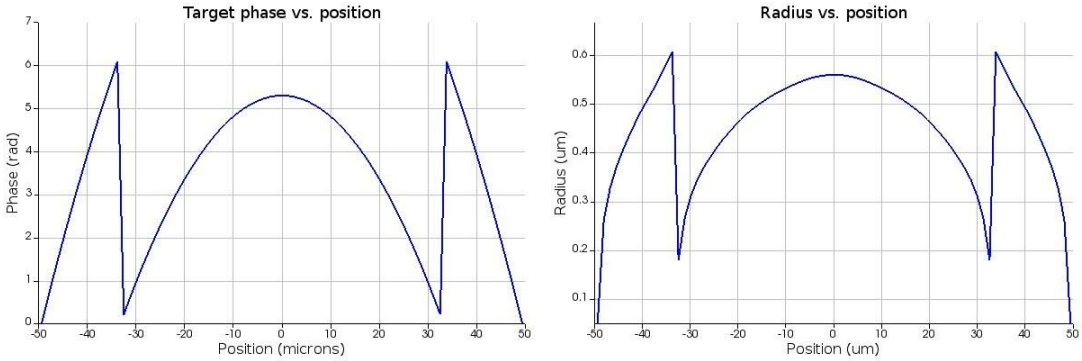

Figure 5. Plots of relation relationships among target phase, position, and radius for plane wave.

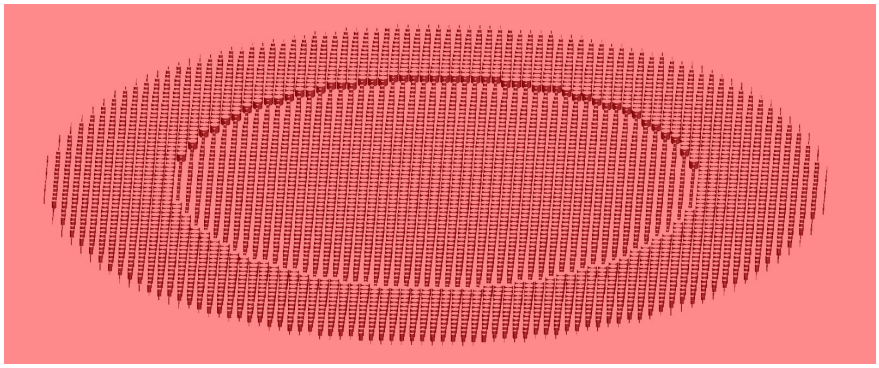

Figure 6. 3D structure of metalens.

The relation between target phase and position is calculated using the above equation and then locations of each nanorod are confirmed by FDTD Lumerical. Finally, the nanorods producing specific phases resulting from different radii are placed at a given position to form a convex metalens as shown in figure 5. Below shows the near-field profile of the convex metalens.

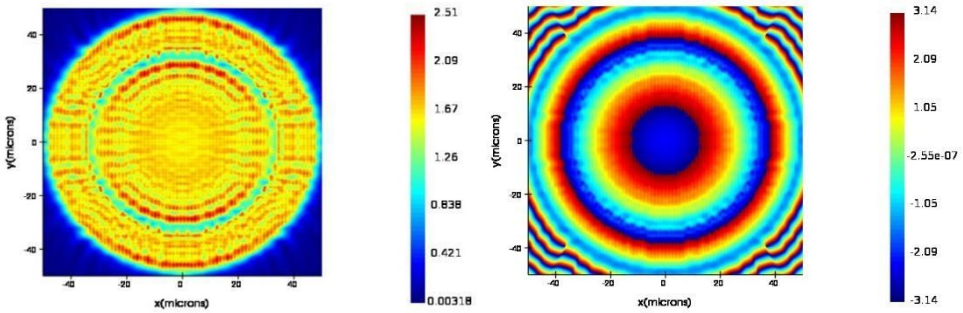

Figure 7. 2D Plots of amplitude (Ex) and phase (Ex) in x-y plane, respectively. The left is a 2D plot of amplitude. The right is a 2D plot of phase.

As shown in figure 6, the shape of the measured phase is the same as the target phase. The only difference is that the measured phase shifts above for a few rads. The reason is that there is a gap between the field monitor and the top of metalens, which inducing a phase change. If the monitor is placed right at the top of the nanorod, the gap between two curves will disappear.

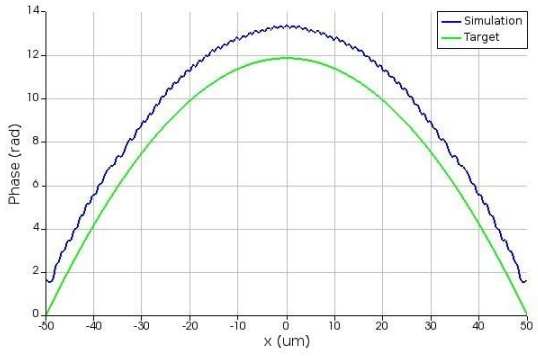

Figure 8. Plots of measured and target phase.

As can be seen from figure 7, the focal length of designed metalens are approximately $148\mu m$. The diameter of spot is $148\mu m$ which are much smaller than the diameter of initial light. Thus, the designed metalens achieved the target to converge the plane wave.

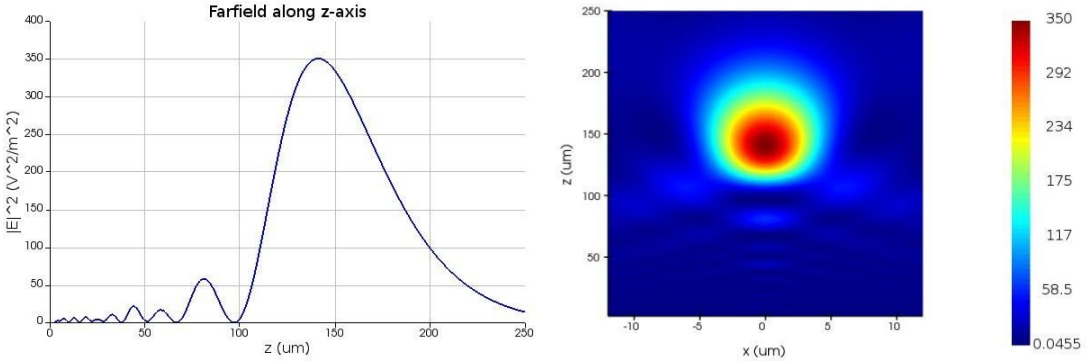

Figure 9. Plots of intensity of far-field. The left is the plot of intensity along z-axis. The right is the 2D map of intensity in x-z plane.

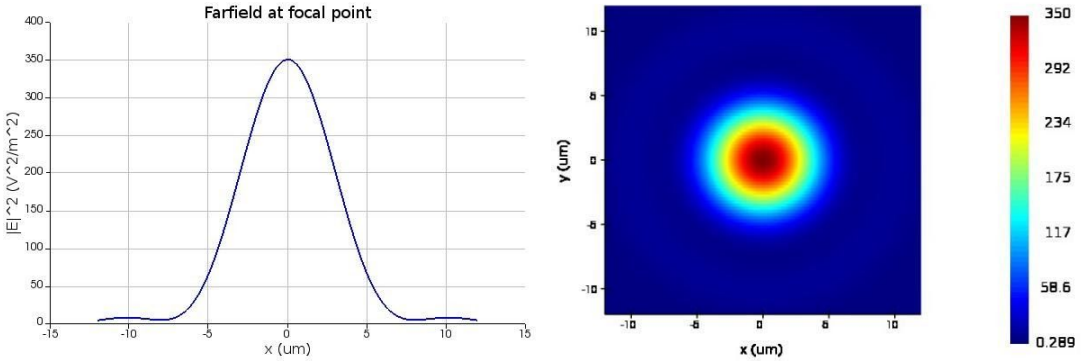

Figure 10. Plots of intensity of far-field at focal point (Left) and 2D map of intensity in x-y plane.

4. Metalens designed for collimating and steering gaussian beam

In this part, metalens are designed to collimate the gaussian beam. After that, the direction of the gaussian beam is controlled by metalens. The following diagram demonstrates the beam path to collimate the gaussian beam.

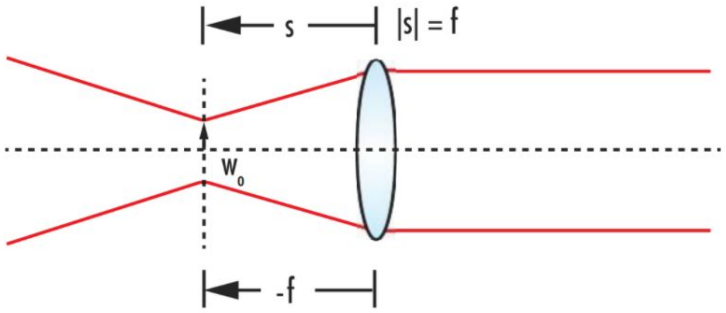

Figure 11. Diagram of collimating gaussian beam.

To collimate a Gaussian beam, the focal length of metalens is supposed to be equal to the distance from the collimating lens and beam waist. Based on this, the equations of distribution of target phase for designing a convex lens can be derived as shown below.

$$\varphi(x,y) = -\frac{\pi x^2}{\lambda f}$$

where

$\lambda = 4.3\mu m$

φ : *phase on the metalens surface*

f : *focal length*

x, y : *spatial coordinates with respect to the center of the lens*

As for the estimated value of focal length of a convex lens, it can be calculated based on lens equation.

$$\frac{1}{f} = \frac{1}{z_1} + \frac{1}{z_2}$$

$$z_1 = \frac{d}{n_{S\square}}$$

where

f : *estimated focal length*

z_1 : *object distance*

z_2 : *image distance, which is positive infinity*

d : *distance from waist*

$n_{S\square}$: *refractive index of Si, which is* 3.88.

By repeating the above procedures designing a convex lens for plane waves, relations among target phase, radius, and position are plots in figure 10. The 3D structure of metalens is shown in figure 13.

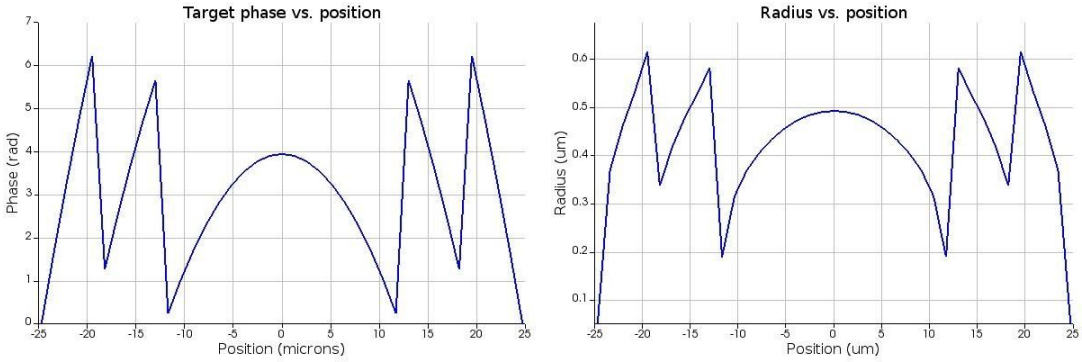

Figure 12. Plots of relation relationships among target phase, position, and radius for gaussian beam.

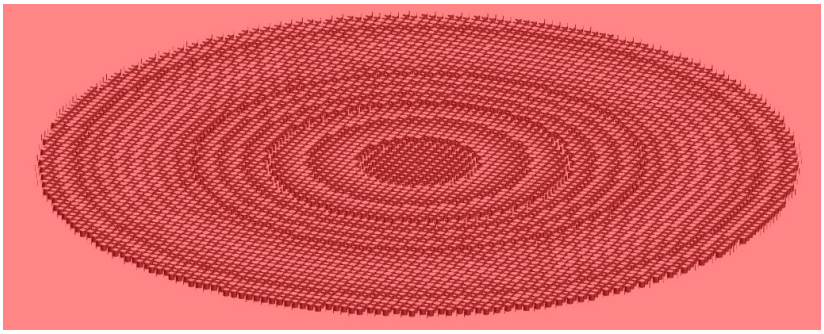

Figure 13. 3D structure of metalens with the center right at the original point.

Below is the 2D plot of amplitude and phase in x-y plane. It's obvious that the diameter of spot is around $20\mu m$, which is much larger than the diameter of light passing through the metalens as shown in figure 15. Thus, the metalens prevents the divergence of the gaussian beam, to some extent.

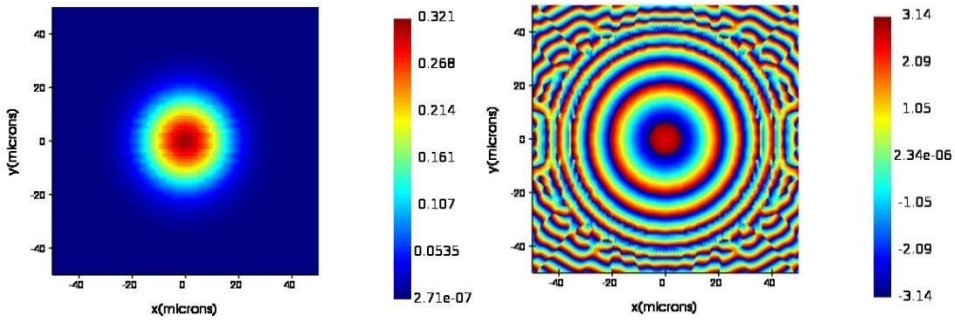

Figure 14. 2D Plots of amplitude (Ex) and phase (Ex) in x-y plane, respectively. The left is a 2D plot of amplitude. The right is a 2D plot of phase.

Figure 15 is the distribution of intensity of the beam along the z-axis. After passing the metalens, the gaussian beam becomes stronger for directional transmission, which means the beam has been collimated.

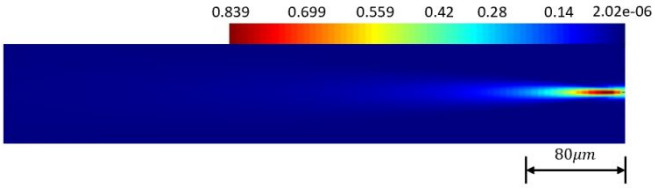

Figure 15. 2D map of intensity of the far-field projection along the z-axis.

Then, the direction of the beam is controlled by shifting the center of the metalens from the original point as shown in figure 16. In the following image, the value of offset between the center of the metalens and original point is 20μm.

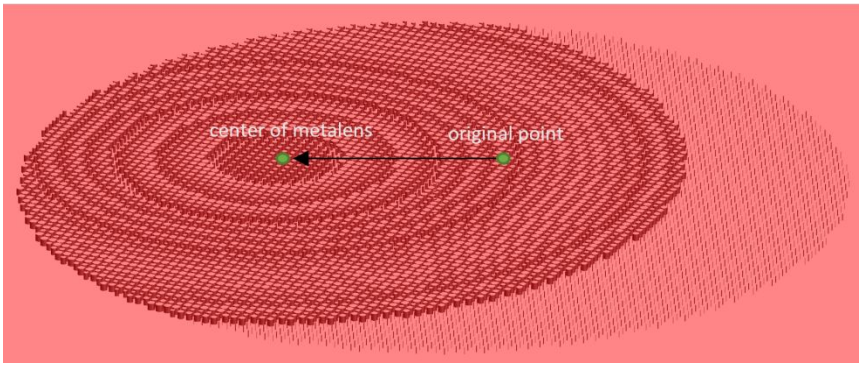

Figure 16. 3D structure of metalens with the center shifting 20μm from original point.

By adjusting the value of offset between the center of the metalens and original point, the direction of the beam is controlled and the deflected angle of each beam is calculated as shown in figure 15.

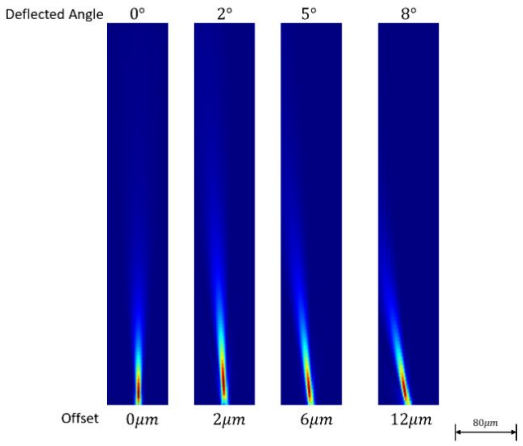

Figure 17. 2D map of the far-field projection along the z-axis with different offset values from the original point.

References

1. N. Yu, L. Diehl, E. Cubukcu, D. Bour, S. Corzine, G. Höfler, A. K. Wojcik, K. B. Crozier, A. Belyanin, and F. Capasso, “Coherent Coupling of Multiple Transverse Modes in Quantum Cascade Lasers,” Phys. Rev. Lett. **102**(1), 013901 (2009).
2. FDTD Lumerical knowledge base.
3. Yi-Yang Xie, Pei-Nan Ni, and Qiu-Hua Wang,“Metasurface-integrated vertical cavity surface-emitting lasers for programmable directional lasing emissions” Nature Nanotechnology, Vol 5, February 2020, 125-130.
4. Xiao Han, Ziyang Fan, Zeyang Liu, Chao Li, and L.Jay Guo,“Inverse design of metasurface optical filters using deep neural networks with high degrees of freedom,” DOI: 10.1002/inf2.12116.
5. Qingbin Fan, Mingze Liu, Cheng Yang, and Ting Xu, “A high numerical aperture, polarization insensitive metalens for long-wavelength infrared imaging,” Appl.Phys.Lett. 113, 201104(2018).